Research Article Vol. 32, No. 4 / 12 Feb 2024 / Optics Express 5492
Optics EXPRESS

Broadband and robust Mach-Zehnder interferometer for Rydberg atomic system

QINGHUI LI,[1] MINGJIAN JU,[1] XIN SHANG,[1] ZHENGLEI MA,[1] WEI LI,[1,2,4] YAJUN WANG,[1,2] LIRONG CHEN,[1,2] LINJIE ZHANG,[2,3] PENGFEI ZHANG,[1,2] AND YAOHUI ZHENG[1,2,5]

[1]*State Key Laboratory of Quantum Optics and Quantum Optics Devices, Institute of Opto-Electronics, Shanxi University, Taiyuan 030006, China*
[2]*Collaborative Innovation Center of Extreme Optics, Shanxi University, Taiyuan 030006, China*
[3]*State Key Laboratory of Quantum Optics and Quantum Optics Devices, Institute of Laser Spectroscopy, Shanxi University, Taiyuan, Shanxi 030006, China*
[4]*xliwei@sxu.edu.cn*
[5]*yhzheng@sxu.edu.cn*

Abstract: We present a broadband and robust Mach-Zehnder interferometer (MZI) with meter-scale arm length, aiming to acquire the full information of an atomic system. We utilize a pre-loading phase shifter as servo actuator, broadening the servo bandwidth to 108 kHz without sacrificing the size of the piezoelectric transducer (PZT) and mirror. An auxiliary laser at 780 nm, counter-propagating with the probe laser, is employed to achieve arbitrary phase locking of the MZI, boosting a phase accuracy of 0.45 degrees and an Allan deviation of 0.015 degrees, which breaks the current record. By utilizing our robust MZI, the measurement accuracy of atomic system can be theoretically predicted to improve by 2.3 times compared to the most stable MZI in other literatures. In addition, we also demonstrate the sensitivity improvement in imaginary part and real part of the susceptibility in virtue of the completed interferometer, which exhibits tremendous potential in atom-based measurement system.

1. Introduction

The Rydberg atomic system emerges as a highly promising platform for microwave electric field sensing, distinguished by its remarkable sensitivity and spatial resolution [1–8]. The core principle is to readout the interaction effect between microwave electric field and Rydberg atoms by electromagnetically induced transparency (EIT) [9,10]. Historically, the majority of research efforts have focused solely on atomic absorption, employing direct optical readout. To access information related to atomic dispersion, the construction of a Mach-Zehnder interferometer (MZI) [11–15] is necessary, with the additional requirement of locking the relative phase to $\pi/2$ [16]. The demonstration further confirms that the MZI with long-term control has a tremendous potential for Rydberg radars where the microwave signals are unknown [17–19]. Recently, by the employment of a MZI, W. G. Yang et al. demonstrated not only the enhanced sensitivity of atom-based microwave-field electrometry, but also the simultaneous measurement of the atomic absorption and dispersion signal [20]. However, the arbitrary phase control of the MZI in the literature relies on the orthogonal polarization of the probe laser, the crosstalk between two polarization beams limits locking performance.

The readout frequency is another important parameter of affecting measurement sensitivity. On one hand, the desired signal gets weaker at above 100 kHz [21]. On the other hand, the readout noise of atomic superhet is increased obviously by light-atom interaction when the frequency is larger than 100 kHz, while there is a tradeoff between the probe laser noise and light-atom interaction noise in the frequency region of 0.1-100 kHz [22]. A mode cleaner, which

#513946 https://doi.org/10.1364/OE.513946
Journal © 2024 Received 21 Nov 2023; revised 21 Dec 2023; accepted 2 Jan 2024; published 31 Jan 2024

Optics EXPRESS

is an optical low-pass filter, can be used to suppress the probe noise at higher frequency band. However, the noise suppression becomes more and more difficult as the frequency reduces. In summary, 100 kHz is a popular frequency to optimize the detection sensitivity, without increasing system complexity. Therefore, we hope to construct a robust MZI with the servo bandwidth of 100 kHz scale. To obtain a broadband servo system, various phase shifter structures have been demonstrated. T. Briles et al. introduced a copper-shielded lead complex structure with a 180 kHz feedback bandwidth [23]. A. Chadi et al. held their piezoelectric transducer (PZT) via a side-clamping, achieving a bandwidth of 100 kHz [24]. D. Goldovsky et al. demonstrated a servo bandwidth of approximately 200 kHz using straightforward elastic rubber rings [25]. T. Nakamura et al. showcased an effective feedback bandwidth of 500 kHz through the utilization of a wedged damping alloy [26]. It's worth mentioning that the increased bandwidth is achieved at the expense of reducing the size of both the PZT and the mirror, which inevitably limit the displacement of PZT to very small. To accommodate the microwave-shielding atomic system, there needs a large-size MZI. Unfortunately, the small PZT is not enough to meet the requirement for the displacement.

In recent years, significant efforts have been dedicated to enhancing the phase stability of interferometers. D. Grassani et al. reported their success in maintaining stable locking of a Michelson interferometer (7 cm×17 cm) at arbitrary phase angle with a precision exceeding 1 degree [27]. M. Micuda et al. showcased a Sagnac interferometer (27 cm×40 cm), revealing phase deviations of less than 0.4 degrees over a 250-second measurement period without any active stabilization [28]. S. H. Wu et al. achieved precise, rapid, and enduring locking MZI at any desired phase point, with phase lock accuracy controllable to within 1.05 degrees [29]. X. X. Ma et al. demonstrated remarkable phase locking performance in an MZI, with an Allan deviation of only 0.026 degrees in 30 minutes [30]. It is eternal pursuit of continuously improving the phase locking accuracy, as well as extending the servo bandwidth under the premise of guaranteeing enough size.

In this paper, we present the realization of a broadband and exceptionally stable MZI with the arm length of meter-scale. In virtue of a "rubber ring1-PZT-mirror-rubber ring2" phase shifter structure, named as pre-loading structure, the servo bandwidth is extended to 108 kHz without sacrificing the size of the PZT and mirror. Thanks to the application of the large-size PZT and mirror, the variation of the arm satisfies the need of meter-scale interferometer. In addition, by the employment of an auxiliary laser that has different wavelength with the probe laser, the crosstalk between two polarization beams is significantly eliminated, leading to a remarkable reduction in phase deviation. As the results, the phase accuracy is 0.45 degrees and the Allan deviation is only 0.015 degrees, which is to our knowledge the best results of meter-scale interferometer. Finally, the completed MZI is utilized to a practical atom-based measurement system, demonstrating the obvious sensitivity improvement comparing with no interferometer case.

2. Broadband and stable phase shifter

The servo bandwidth is primarily influenced by the structure of the phase shifter and the individual bandwidth of components within the feedback loop. Figure 1 illustrates the schematic of our homemade phase shifter. For this purpose, we employed a multi-stack piezoelectric cylinder P-010.00P from PI, capable of providing a 5 μm displacement for 1000 V applied. The masses of PZT and mirror are 6 g and 0.42 g respectively, while the mount, crafted from copper, weighs approximately 1.5 kg. To enhance the system's performance, we've integrated two nitrile rubber rings, renowned for their excellent elasticity, serving as springs. In this way, the net displacement of mirror will be determined by the stiffness ratio between the back rubber ring and the front ring. These rings effectively isolate mechanical vibrations originating from the mount and the optical table, thereby significantly broadening the servo bandwidth.

Optics EXPRESS

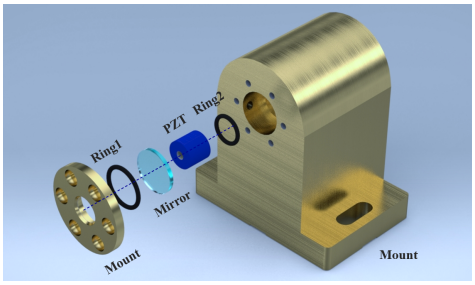

Fig. 1. Schematic illustration of the phase shifter. The size of rubber ring1 is 12.7 mm (diameter) × 1.5 mm (thickness), the size of rubber ring2 is 10 mm (diameter) × 1.5 mm (thickness), the size of mirror is 12.7mm (diameter) × 1.5 mm (thickness), and the size of PZT is 10 mm (diameter) × 9 mm (length).

The transfer function of servo system is acquired through the utilization of the Moku: Lab frequency response analyzer, as depicted in Fig. 2. In Fig. 2(a) and Fig. 2(b), we illustrate the amplitude and phase responses of our servo system. In accordance with the definition of servo bandwidth [31], which is the frequency point where the closed-loop amplitude response reaches -3 dB, the servo bandwidth of our feedback system is identified to be 108 kHz. Furthermore, this servo bandwidth can also be derived from the frequency point at which the phase response undergoes a shift of -180°, which is in accordance with above results. It is worth emphasizing that the bandwidth of the photodetector stands at 1 MHz, the high-voltage amplifier (HV-amp) exhibits a bandwidth of 420 kHz, the proportional integral differentiator (PID) demonstrates a bandwidth of 110 kHz, and the PZT resonance frequency is registered at 129 kHz. Consequently, the servo bandwidth is principally limited by the resonance frequency of the PZT.

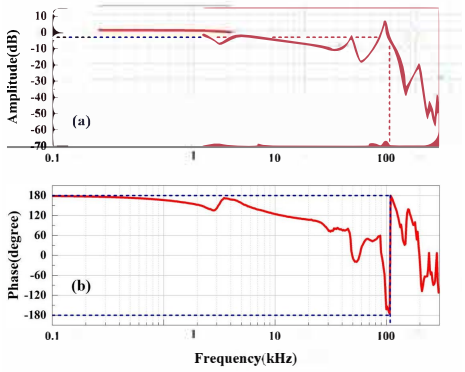

Fig. 2. The frequency response of servo system in both amplitude (a) and phase (b). The sweep frequency of sine output is 100 Hz-1 MHz and 512 points per sweep are selected.

3. Stable MZI

The experimental configuration of the MZI (50 cm × 25 cm) is illustrated in Fig. 3. The probe laser, operating at 852 nm (Toptica, DL PRO) is efficiently coupled from a polarization-maintaining fiber into free space through a collimator (PAF2-7B). The probe laser (red solid line) is divided into two beams via a 50:50 beam splitter1 (BS1). The transmission beam passes through a neutral density filter (NDF) and subsequently interacts with the atomic vapor, assuming the role of a

Optics EXPRESS

weak signal. Simultaneously, the reflected beam serves as a strong local oscillator. These two optical pathways are overlapped together on beam splitter2 (BS2) with an interference contrast exceeding 99%, and then is captured by a balanced homodyne detector (BHD). In this way, not only the technical noise of probe laser is subtracted by BHD, but the weak signal is amplified by local oscillator. Additionally, the coupling laser at 510 nm (green dash line) counter propagates along the signal beam, interacting with the atomic vapor.

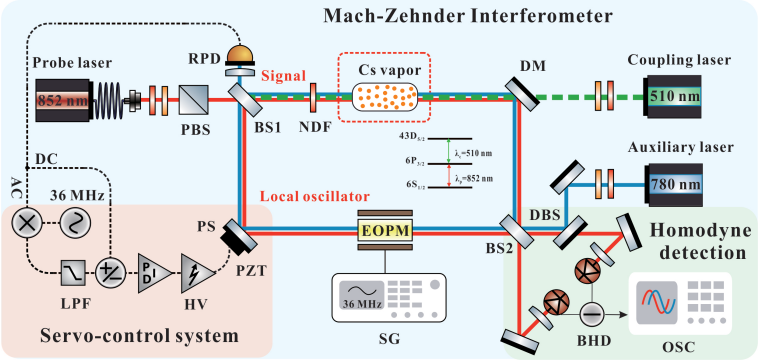

Fig. 3. The experimental setup of Mach-Zehnder interferometer. BS: beam splitter; NDF: neutral density filter; DM: dichroic mirror; DBS: dichroic beam splitter; PS: phase shifter; PZT: piezoelectric transducer; EOPM: electro-optical phase modulator; RPD: resonant photodetector; BHD: balanced homodyne detection; OSC: oscilloscope; SG: signal generator.

An auxiliary locking laser at 780 nm (blue solid line) enters the MZI via BS2 and counter propagates through the interferometer. Importantly, the locking laser does not interact with the atomic vapor, ensuring minimal crosstalk with the signal light. The homemade phase shifter, positioned in the path of local oscillator, is used to control the relative phase between two arms of MZI. To control the signal and local oscillator in phase, local oscillator undergoes phase modulation at a fixed frequency, typically set at 36 MHz, which is achieved using an electro-optical phase modulator (EOPM). Subsequently, the output of the locking laser within the MZI is captured by a resonant photodetector (RPD), demodulated to extract the PDH error signal [32]. The relative phase between the signal and local oscillator is actively locked to $\pi/2$ by utilizing the interference error signal. By superposing the PDH error signal with the interference error signal in a specific proportion, the MZI can be precisely controlled to an arbitrary phase.

The phase locking stability relies on the mechanical stability and the performance of the RPD, PID and HV-amp systems. The mechanical structure of phase shifter with integrated and large base area significantly diminishes phase uncertainty during experimental procedures. The RPD incorporates an inductance capacitance (LC) resonance circuit, acting as a band-pass filter, which amplifies the signal at the resonance frequency while attenuating noise outside the bandwidth. The actual resonant frequency (36 MHz) can be fine-tuned by adjusting the value of inductor L [33–36]. Then one can extract an error signal with high signal-to-noise ratio (SNR), ensuring stable locking of the MZI. The PID employs a cascade structure, an active twin-T notch filter and a low-pass filter. The twin-T notch filter is used to remove unnecessary resonances with tunable attenuation and quality factor, whereas the low-pass filter suppresses high-frequency vibration outside the bandwidth. In this experiment, the integrator and low-pass filter were configured with cutoff frequencies of 3 kHz and 110 kHz, respectively. The locking stability is boosted by suppressing a majority of disturbance within the bandwidth. To prevent distortion of the PID control signal and enable synchronous response to high-frequency control signals, the HV-amp utilizes the power amplifier chip PA98, which affords an operational bandwidth of 420 kHz during full-power operation (375±10 V).

Optics EXPRESS

To verify the optimization effect of the experimental system, we measure the locking stability in time domain when the relative phase between signal beam and local oscillator is locked to 0. The direct current (DC) output from the BHD is split into two segments, one of which is connected to a digital oscilloscope for real-time DC monitoring, providing immediate insights into the locking stability. Simultaneously, the other segment is introduced into a high-precision digital multimeter, specifically the Keithley 3706A, and the data is recorded in real time over an extended period.

Figure 4(a) illustrate the experimental results, from which the stability of the phase shift within the interferometer can be deduced. The inset is a phase distribution histogram and the phase accuracy is 0.45 deg within 97.52%. Figure 4(b) shows the Allan deviation of the phase shift over 2 hours. When the averaging time reaches 512 seconds, the stability of the phase shift reduces to 0.015 degrees, equivalent to 2.62×10^{-4} rad. This level of precision corresponds to an interferometer arm length deviation of 0.0355 nm ($4.2 \times 10^{-5}\lambda$), or a relative length deviation of 4.73×10^{-11}. When the averaging time surpasses 512 seconds, the influence of low-frequency fluctuations in the laboratory environment gradually becomes apparent. It is worth emphasizing that this configuration enables us to perform exceptionally stable measurements over an extended duration, making it especially suitable for applications involving Rydberg atoms.

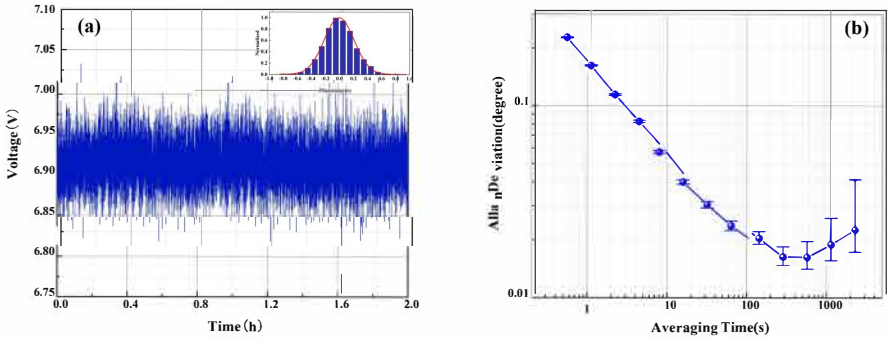

Fig. 4. (a) The measured phase fluctuation of MZI. (b) The Allan deviation of the phase shift.

4. Application to atomic vapors

Utilizing the configuration described above, we introduce cesium (Cs) vapor into the signal arm of the interferometer, thus the 852 nm and 510 nm lasers act as the probe laser and the coupling laser respectively, generating the EIT effect. The energy level diagram of Cs atoms is illustrated in Fig. 3, where $6S_{1/2}$ is the ground state, $6P_{3/2}$ is the intermediate state, and $43D_{5/2}$ is the Rydberg state. This setup allows us to explore and quantify the amplification effect of the imaginary part and real part of the susceptibility, enabling us to extract the full information related to the atomic response.

The EIT transmission signal can be analyzed with an oscilloscope, the optical readout signal is represented by the following expression [20]

$$I = a\cos(\Delta\phi + \Delta\theta) \tag{1}$$

$$a \propto \exp\left\{\frac{-2\pi l\,\mathrm{Im}[\chi]}{\lambda_p}\right\} \tag{2}$$

Optics EXPRESS

$$\Delta\phi \propto \frac{\pi l \,\mathrm{Re}[\chi]}{\lambda_p} \tag{3}$$

where the parameter a represents the transmission loss, $\Delta\phi$ is the phase shift induced by the dispersion of light in Cs vapor, $\Delta\theta$ is the relative phase between the signal and local oscillator, l signifies the length of the Cs vapor, λ_p represents the probe laser wavelength, and χ is the complex susceptibility of the Cs vapor. When the relative phase between signal and local oscillator is actively locked at 0, this configuration allows for the measurement of the imaginary part of the susceptibility, which, in turn, provides critical information about the absorption properties of the Cs atoms. By locking the relative phase between the signal and local oscillator to $\pi/2$, the real part of the susceptibility that is the dispersion information of the Cs atoms is recorded. This approach enables a thorough exploration of both the imaginary part and real part of the susceptibility associated with the atomic response. Moreover, for definite atomic response, the accuracy for readout signal is proportional to the phase locking accuracy for MZI. By utilizing our robust MZI, the measurement accuracy of atomic system can be predicted to improve by 2.3 times compared to the MZI with phase accuracy of 1.05 degrees.

Setting the signal power to 20 μW, the imaginary part of the susceptibility is direct recorded and displayed in Fig. 5(a) (the black curve). Then we measure the imaginary part of susceptibility by controlling the relative phase of MZI to 0. When the power of signal beam remains at 20 μW and the power of local oscillator is adjusted to 0.5 mW, the imaginary part of the susceptibility is enlarged by 18 times, represented by purple curve. Adjusting the power of local oscillator to 1 mW (2 mW), the imaginary part of the susceptibility is shown by the blue (red) curve, and magnified by 23 (29) times. The signal magnification is linear to the amplitude of the local oscillator [16], as shown in the inset of Fig. 5(a). The real part of the susceptibility is acquired by controlling the relative phase of MZI to $\pi/2$, depicted as green curves in Fig. 5(b). Obviously, both the imaginary part and real part of the susceptibility are measured with high sensitivity in virtue of the robust and broadband MZI.

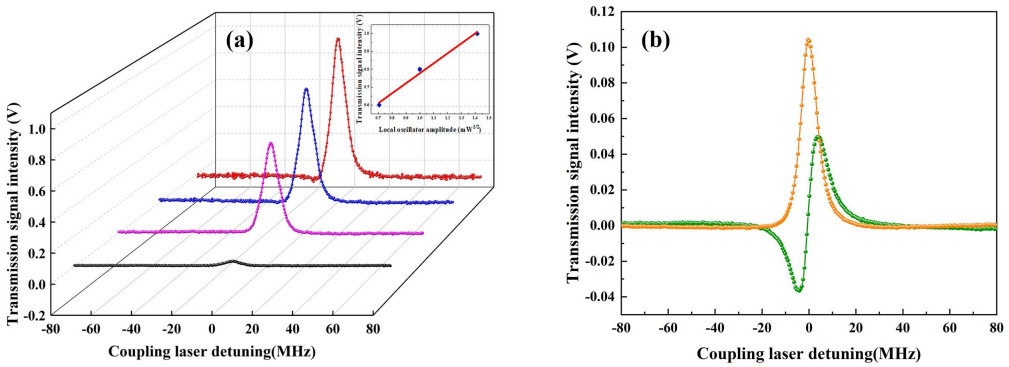

Fig. 5. (a) The measurement results via direct readout (black curve) and MZI (purple, blue and red curves). (b) The imaginary part (orange curve) and real part (green curve) of the susceptibility measured by MZI.

Optics EXPRESS

5. Conclusion

We have presented the demonstration of a broadband and exceptionally stable MZI with the arm length of meter-scale. By tailoring the "rubber ring1-PZT-mirror-rubber ring2" phase shifter structure, the servo bandwidth is significantly broadened to 108 kHz without sacrificing the size of PZT and mirror. The phase control of MZI is achieved by introducing an auxiliary laser that counter propagates alongside the probe laser, leading to a remarkable reduction in phase deviation. With a continuously operating time for over 2 hours, the phase accuracy is 0.45 degrees and the Allan deviation is only 0.015 degrees. Compared to the MZI with phase accuracy of 1.05 degrees, the measurement accuracy of atomic system can be theoretically predicted to improve by 2.3 times with the robust and broadband MZI. It can be extensively applied to enhance the sensitivity and resolution of microwave electric field sensing in atom-based system.

Funding. National Natural Science Foundation of China (62225504, 62027821, U22A6003, 12274275, 62375162); National Key Research and Development Program of China (2020YFC2200402); Key Research and Development Program of Shanxi (202102150101003 .

Disclosures. The authors declare no conflicts of interest.

Data availability. Data underlying the results presented in this paper are not publicly available at this time but may be obtained from the authors upon reasonable request.

References

1. Y. Cui, F. Jia, J. Hao, *et al.*, "Extending bandwidth sensitivity of Rydberg-atom-based microwave electrometry using an auxiliary microwave field," Phys. Rev. A **107**(4), 043102 (2023).
2. B. Liu, L. Zhang, Z. Liu, *et al.*, "Highly sensitive measurement of a megahertz RF electric field with a Rydberg-atom sensor," Phys. Rev. A **18**(1), 014045 (2022).
3. L. Zhang, Z. Liu, B. Liu, *et al.*, "Rydberg microwave-frequency-comb spectrometer," Phys. Rev. A **18**(1), 014033 (2022).
4. M. Cai, Z. Xu, S. You, *et al.*, "Sensitivity Improvement and Determination of Rydberg Atom-Based Microwave Sensor," Photonics **9**(4), 250 (2022).
5. M. Jing, Y. Hu, J. Ma, *et al.*, "Atomic superheterodyne receiver based on microwave-dressed Rydberg spectroscopy," Nat. Phys. **16**(9), 911–915 (2020).
6. J. Yuan, W. Yang, M. Jing, *et al.*, "Quantum sensing of microwave electric fields based on Rydberg atoms," Rep. Prog. Phys. **86**(10), 106001 (2023).
7. J. Hu, H. Li, R. Song, *et al.*, "Continuously tunable radio frequency electrometry with Rydberg atoms," Appl. Phys. Lett. **121**(1), 014002 (2022).
8. N. Prajapati, A. Robinson, S. Berweger, *et al.*, "Enhancement of electromagnetically induced transparency based Rydberg-atom electrometry through population repumping," Appl. Phys. Lett. **119**(21), 214001 (2021).
9. J. Sedlacek, A. Schwettmann, H. Kübler, *et al.*, "Microwave electrometry with Rydberg atoms in a vapor cell using bright atomic resonances," Nat. Phys. **8**(11), 819–824 (2012).
10. M. Simons, J. Gordon, C. Holloway, *et al.*, "Using frequency detuning to improve the sensitivity of electric field measurements via electromagnetically induced transparency and Autler-Townes splitting in Rydberg atoms," Appl. Phys. Lett. **108**(17), 174101 (2016).
11. S. Kumar, H. Fan, H. Kübler, *et al.*, "Atom-Based Sensing of Weak Radio Frequency Electric Fields Using Homodyne Readout," Sci. Rep. **7**(1), 42981 (2017).
12. S. Aljunid, M. Tey, B. Chng, *et al.*, "Phase Shift of aWeak Coherent Beam Induced by a Single Atom," Phys. Rev. Lett. **103**(15), 153601 (2009).
13. W. Oliver, Y. Yu, J. Lee, *et al.*, "Mach-Zehnder interferometry in a strongly driven superconducting qubit," Science **310**(5754), 1653–1657 (2005).
14. M. Armen, J. Au, J. Stockton, *et al.*, "Adaptive homodyne measurement of optical phase," Phys. Rev. Lett. **89**(13), 133602 (2002).
15. M. Scully and M. Fleischhauer, "High-sensitivity magnetometer based on index-enhanced media," Phys. Rev. Lett. **69**(9), 1360–1363 (1992).
16. M. Xiao, Y. Li, S. Jin, *et al.*, "Measurement of dispersive properties of electromagnetically induced transparency in rubidium atoms," Phys. Rev. Lett. **74**(5), 666–669 (1995).
17. A. Robinson, N. Prajapati, D. Senic, *et al.*, "Determining the angle-of-arrival of a radio-frequency source with a Rydberg atom-based sensor," Appl. Phys. Lett. **118**(11), 114001 (2021).
18. C. Fancher, D. Scherer, M. John, *et al.*, "Rydberg Atom Electric Field Sensors for Communications and Sensing," IEEE Trans. Quantum Eng. **2**, 1–13 (2021).
19. J. Sedlacek, A. Schwettmann, H. Kübler, *et al.*, "Atom-Based Vector Microwave Electrometry Using Rubidium Rydberg Atoms in a Vapor Cell," Phys. Rev. Lett. **111**(6), 063001 (2013).

Optics EXPRESS

20. W. Yang, M. Jing, H. Zhang, *et al.*, "Enhancing the Sensitivity of Atom-Based Microwave-Field Electrometry Using a Mach-Zehnder Interferometer," Phys. Rev. Appl. **19**(6), 064021 (2023).
21. M. Simons, A. Haddab, J. Gordon, *et al.*, "A Rydberg atom-based mixer: Measuring the phase of a radio frequency wave," Appl. Phys. Lett. **114**(11), 114101 (2019).
22. Z. Wang, M. Jing, P. Zhang, *et al.*, "Noise analysis of the atomic superheterodyne receiver based on flat-top laser beams," Opt. Express **31**(12), 19909-19917 (2023).
23. T. Briles, D. Yost, A. Cingöz, *et al.*, "Simple piezoelectric-actuated mirror with 180 kHz servo bandwidth," Opt. Express **18**(10), 9739–9746 (2010).
24. A. Chadi, G. Méjean, R. Grilli, *et al.*, "Note: Simple and compact piezoelectric mirror actuator with 100 kHz bandwidth, using standard components," Rev. Sci. Instrum. **84**(5), 56112–56113 (2013).
25. D. Goldovsky, V. Jouravsky, and A. Pe'er, "Simple and robust phase-locking of optical cavities with > 200 KHz servo-bandwidth using a piezo-actuated mirror mounted in soft materials," Opt. Express **24**(25), 28239–28246 (2016).
26. T. Nakamura, S. Tani, I. Ito, *et al.*, "Piezo-electric transducer actuated mirror with a servo bandwidth beyond 500 kHz," Opt. Express **28**(11), 16118-16125 (2020).
27. D. Grassani, M. Galli, and D. Bajoni, "Active stabilization of a Michelson interferometer at an arbitrary phase with subnanometer resolution," Opt. Lett. **39**(8), 2530–2533 (2014).
28. M. Micuda, E. Dolakova, I. Straka, *et al.*, "Highly stable polarization independent Mach-Zehnder interferometer," Rev. Sci. Instrum. **85**(8), 083103 (2014).
29. S. Wu, W. Huang, P. Yang, *et al.*, "Arbitrary phase-locking in Mach–Zehnder interferometer," Opt. Commun. **442**(3), 148–151 (2019).
30. X. Ma, X. Zhang, K. Huang, *et al.*, "Noise-suppressing and lock-free optical interferometer for cold atom experiments," Opt. Express **28**(19), 28584-28589 (2020).
31. C. Zhang, R. Li, W. Zhang, *et al.*, "Experimental study on noise characteristics of audio frequency band in output field of optical filter cavity," Acta Phys. Sin. **71**(24), 244205 (2022).
32. E. Black, "An introduction to Pound–Drever–Hall laser frequency stabilization," Am. J. Phys. **69**(1), 79–87 (2001).
33. L. Tian, L. Zheng, X. Zhang, *et al.*, "Resonant electro-optic phase modulator and photodetector for stabilizing laser frequency and quantum optics," Acta Phys. Sin. **72**(14), 148502 (2023).
34. C. Chen, Z. Li, X. Jin, *et al.*, "Resonant photodetector for cavity- and phase-locking of squeezed state generation," Rev. Sci. Instrum. **87**(10), 103114 (2016).
35. C. Chen, S. Shi, and Y. Zheng, "Low-noise, transformer-coupled resonant photodetector for squeezed state generation," Rev. Sci. Instrum. **88**(10), 103101 (2017).
36. H. Zhang, J. Wang, Q. Li, *et al.*, "Experimental realization of high quality factor resonance detector," Journal of Quantum Optics **25**(04), 456–462 (2019).